Experimental Evaluation of the Viscoelasticity of Porcine Vitreous

Ali Aboulatta[1]*, Ahmed Abass[1], Ahmed Makarem[1], Ashkan Eliasy[1], Dong Zhou[1], Duo Chen[2], Xiaoyu Liu[2,3*], Ahmed Elsheikh[1,3-4]

Affiliations

[1] School of Engineering, University of Liverpool, Liverpool, L69 3GH, UK

[2] Key Laboratory for Biomechanics and Mechanobiology of the ministry of Education, School of Biological Science and Medical Engineering, Beihang University, China

[3] Beijing Advanced Innovation Centre for Biomedical Engineering, Beihang University, Beijing, 100083, China

[4] NIHR Biomedical Research Centre for Ophthalmology, Moorfields Eye Hospital NHS Foundation Trust and UCL Institute of Ophthalmology, UK

*** Corresponding Author:**

Ali Aboulatta

School of Engineering, University of Liverpool, Liverpool, L69 3GH, UK,

sgaaboul@liverpool.ac.uk

Xiaoyu Liu

School of Biological Science and Medical Engineering, Beihang University, Beijing, 100191, China

x.y.liu@buaa.edu.cn

Keywords: Eye; Retina; Vitreous; Retinal Detachment; Sclera

Number of words: 5722

Abstract

Purpose: This study aims to estimate the material properties of the porcine vitreous while testing it in close to its natural physiologic conditions.

Methods: Eighteen porcine eyes were tested within 48h post-mortem. A custom-built computer-controlled test rig was designed to support, load and monitor the behaviour of eye globes while being subjected to dynamic rotation cycles mimicking saccade eye movement. Specimens were glued to the base of a container, surrounded by gelatine, frozen and cut in half to expose the vitreous. After thawing, the container was subjected to concentric dynamic rotations of up to 5°, 10° or 15°, while taking 50MP photos of the specimen every 2 ms. The images were analysed by a digital image correlation algorithm to trace the movement of marked points on the vitreous surface with different radii from the centre of the posterior chamber. The initial camera image was used in building a finite element model of the test set up, which was used in an inverse analysis exercise to estimate the material properties of the vitreous.

Results: Angular displacements of the monitored points were up to 3.3°, 4.1° and 3.9° in response to eye rotations of 5°, 10° and 15°, respectively. With the experimental relationships between eye rotation and angular displacements used as target behaviour, the inverse analysis exercise estimated the initial shear modulus, the long-term shear modulus and the viscoelastic decay constant of the porcine vitreous as 2.10±0.15 Pa, 0.50±0.04 Pa and 1.20 ±0.09 s^{-1}, respectively.

Conclusions: Consideration of the viscoelasticity of the vitreous was essential to represent its experimental behaviour. Testing the vitreous in close to its normal physiologic conditions produced estimations of the initial shear modulus and long-term shear modulus that were respectively smaller and larger than reported values [1-3].

1. Introduction

The eye's vitreous humour is a gel-like substance that fills the cavity behind the lens, which constitutes 80% of the eye's volume [4]. The vitreous consists of three parts; the vitreous base, the vitreous core and the peripheral part. All three parts share the same composition with 99% water, 0.9% salts, and 0.1% collagen fibrils [5, 6]. By the time the eye reaches its adult size, approximately 20% of the total vitreous volume would have turned into liquified vitreous [7]. And with ageing, the vitreous has been reported to experience shrinking and liquefaction [8, 9], the cause of which is still not fully understood [10].

The vitreous has several functions including mediating the growth of the eye [7], supporting ocular tissues [11, 12] and maintaining a clear path of light rays to the retina [7]. Deficiencies in the vitreous molecular structure and viscoelastic properties have been reported to increase the risk of developing glaucoma, rhegmatogenous retinal detachment (RRD), retinal tear, retinal oedema, vitreous haemorrhage and choroidal detachment [7, 10, 13]. Moreover, the adhesion of the vitreous to the surrounding ocular structures may make the removal of the vitreous challenging during vitrectomy where the vitreous is to be replaced with silicone oil [5, 14].

There have been several attempts to describe the composition, structure and material properties of the vitreous. Studies investigated the vitreous shear relaxation modulus in order to estimate its viscoelastic behaviour. The studies used techniques that involved subjecting the vitreous to compression [15], explored relaxation of the scattering pattern [16], and used nuclear magnetic resonance [17], cavitation rheology [1] and cleated tools [18] to monitor behaviour. Using finite element modelling to determine the materials parameters has already been successfully applied, in various forms, to ocular tests [19-22]. For instance, Rossi et al. [3, 23] performed inverse analysis on experimental data obtained from test data of eye impact experiments carried out by Delori et al. [24]. While these efforts shed much light on the vitreous behaviour, and the fact that some methods subjected the tissue to non-physiologic conditions led to a wide variation in the shear relaxation modulus reported in the literature. Saccadic eye movement has been modelled in several studies [25-27]; David et al. [28] investigated the vitreous behaviour due to eye movement. They only

compared between a numerical and analytical model of the vitreous. However, no parameters were determined.

This study aims to measure the properties of the vitreous while keeping the tissue and testing it in close to its natural physiologic conditions. Vitreous specimens were tested while remaining in the posterior chamber and being subjected to the dynamic conditions experienced in saccade eye movements. Numerical inverse analysis based on the nonlinear finite element method was then used to estimate the viscoelastic material properties of the vitreous based on its experimental behaviour.

2. Methods

2.1 Specimen preparation

Eighteen Fresh porcine eyes were obtained from a local abattoir and used within 48h post-mortem. To ensure freshness, the eyes were obtained directly after the animals were slaughtered and were washed and all excess connective tissue was removed. The eyes were then transported to the Ocular Biomechanics Laboratory of Beihang University and tested on arrival.

2.2 Test setup

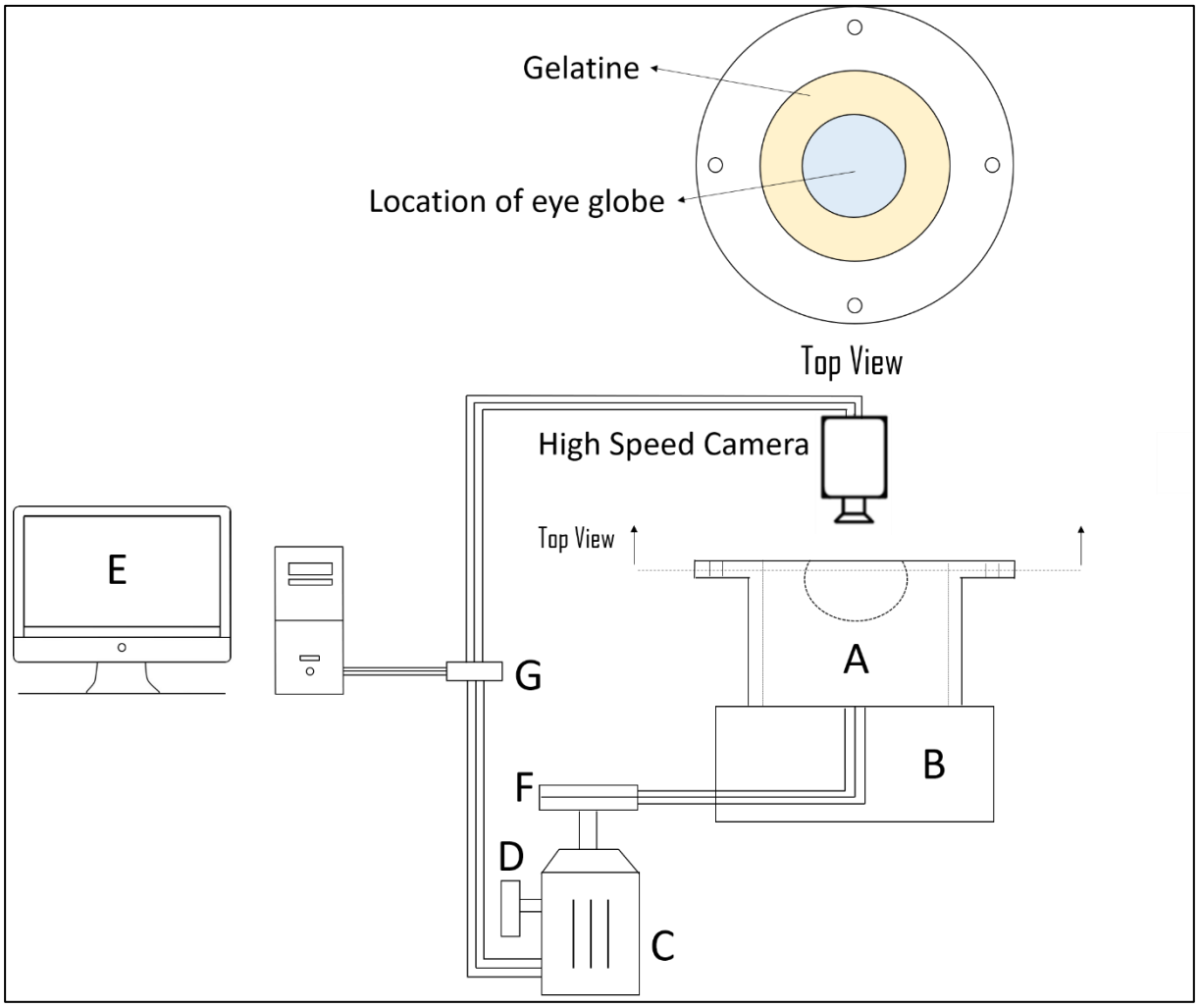

Figure 1 Schematic view of the test rig highlighting key components; where A is the container, B is the metal platform, C is a motor, D is the decelerator, E is a personal computer, F is a reduction gear and G is the data acquisition unit.

A computer-controlled test rig was designed to support, load and monitor the behaviour of eye globes subjected to dynamic rotations representing saccade eye movements, Figure 1. An eye specimen was placed in a container (A in Figure 1), glued to the base using water-based glue (Loctite, Henkel Corporation, Ohio, US) and surrounded by a gelatine material produced from Biowest Agarose (Gene Company Ltd, Chai Wan. Hong Kong). The gelatine was selected based on its material properties which were close to those of the orbital fat that supports the eye in the ocular socket [29] [30]. After

curing the gelatine, the specimen was placed in a freezer at -37ºC for at least a day before being taken out to conduct the test.

The eye globe was then taken out of the freezer and cut in half using a sharp blade moved on the surface of the container, Figure 2. The container was then connected firmly to the centre of a circular metal platform (B in Figure 1) that experienced rotation produced by an electric motor (C), which was able to apply the required loading accelerations. The platform was also connected to a decelerator (D) to reduce the speed as required. High-resolution images of the specimen were taken during the test every 2 ms. The power reaching the motor and the decelerator was controlled by a personal computer (E), which also recorded measurements by the rotation sensor attached to the metal plate and the images taken by the camera.

After the tests, the camera images were analysed using digital image correlation (DIC) software (ProAnalyst, Xcitex, Woburn, Massachusetts, USA) to trace the movement at a number of points on the surface of the vitreous (up to 5 per specimen) selected at different radii from the centre of the posterior chamber. Further, the initial image of the camera, recorded for each specimen, along with eye dimension measurements taken before test, was used in the construction of the specimen-specific finite element model of the test set up (used later in the inverse analysis exercise). The error in the system of measurement was quantified by tracing multiple known positions within the container through DIC, and the resulting RMS error between known positions and their associated measurement was 0.4%. During the quantification tests, all measurements were taken relative to a fixed point, the centre of the container. The DIC technique has already been applied in earlier studies [31, 32], and showed successful results.

As eye movements rarely exceed 15º in amplitude [33], the specimens were subjected to tests with max rotations of either 5º, 10º or 15º. The angular velocity adopted in the tests was also selected to emulate the normal conditions where the saccadic movement duration of the eye is only a function of the angle of eye rotation. An earlier study showed that the angle of rotation ($\propto_o$ in degrees) and duration of rotation (T in seconds) were related according to the equation [34]:

$$T = 0.021 \ \propto_o^{2/5} \qquad \text{Equation 1}$$

Therefore, the angular displacement ($\propto$) and angular velocity (ω) of the saccades adopted in the tests were determined using the relationships [34]:

$$\propto(t) = \frac{\propto_o}{2}\left((1-\cos\left(\frac{\pi}{T}t\right)\right) \quad \text{Equation 2}$$

$$\omega = \frac{\propto_o t}{2T}\sin(\frac{\pi}{T}t) \quad \text{Equation 3}$$

where t is the time at which $\propto$ and ω are calculated.

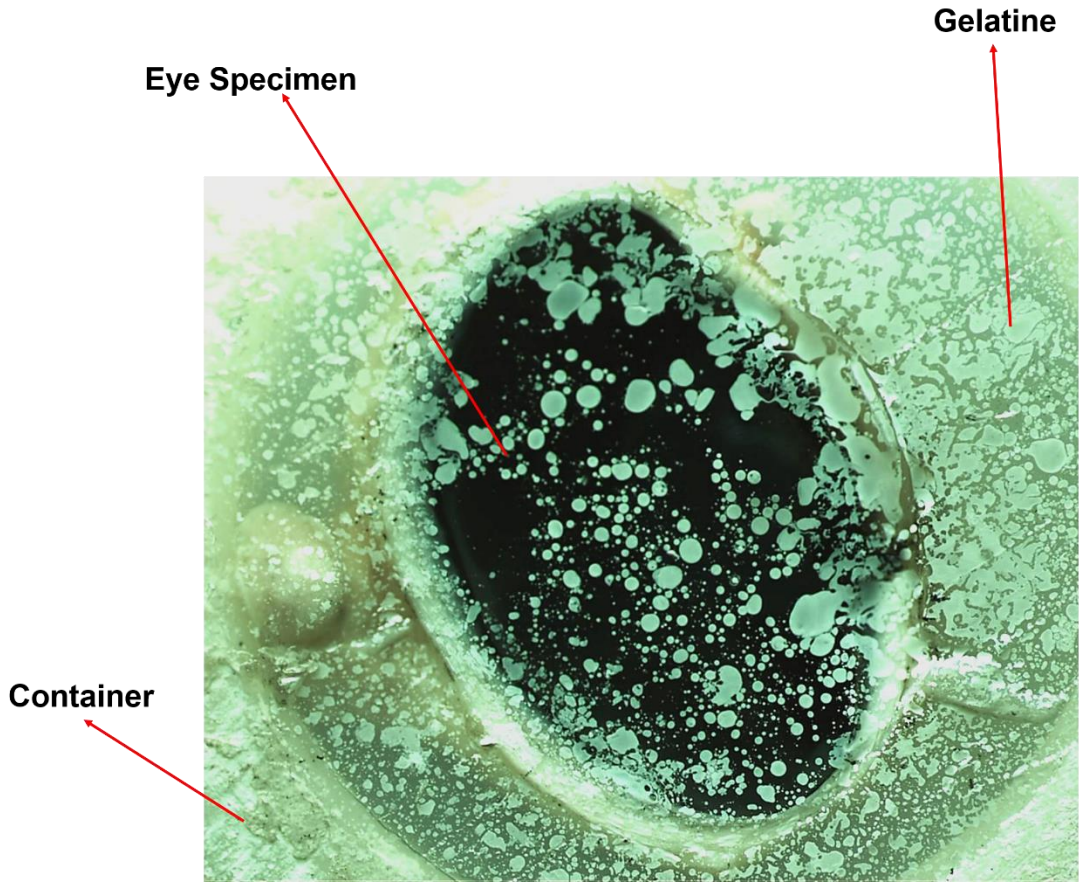

Figure 2 Picture taken of test rig showing an eye specimen, gelatine and container.

2.3 Numerical modelling

A numerical model was built for each specimen for use in the inverse analysis exercise intended to estimate the material behaviour of the vitreous. The model was built for analysis by the commercial finite element analysis (FEA) software ABAQUS (Release 6.14-2, Dassult Systemes, Johnston, Rhode Island, USA). The model included the semi eye globe tested along with the metal container and the gelatine material. The model representing the semi eye included the cornea, limbus, sclera, retina and the

vitreous – it was created using a custom-built MATLAB code (The MathWorks, Inc., Natick, Massachusetts, USA). The specimen-specific model adopted the overall dimensions as captured by the initial camera image, and the measurements taken before the test of corneal size and corneal and scleral thickness.

The cornea and sclera mesh was based on Nooshin and Tomatsuri configuration of diamatic domes [35, 36], and included 3456 6-noded continuum C3D6 elements organised in one layer, and 12 rings in the cornea and 32 rings in the sclera, Figure 3. The sclera elements surrounded a layer of C3D6 elements representing the retina. Inside the retina elements, the vitreous was represented by 20736 C3D6 elements organised in 7 layers and 44 rings. The only exception was the innermost layer of vitreous elements that was formed of tetrahedral elements (type C3D4). The mesh density adopted in the model was the result of a mesh density study to balance accuracy of deformation prediction with the computing time. The mesh convergence study showed a 9.5% change in the deformation of the vitreous when the number of elements increased from 3840 to 24192, while a much smaller change in deformation, of 0.36%, took place when the number of elements increased from 24192 to 110592. Therefore, the model employed 24192 elements were used in the study to represent the vitreous.

The container geometry was modelled in ABAQUS using the dimensions used in the manufacturing process, and the container model was meshed with ABAQUS-CAE automatic meshing tool using quadratic tetrahedron elements (type C3D10). The space between the semi eye globe and the container, filled by the gelatine material, was then meshed. The nodes of the outer layer of the eye model and the inner layer of the container model were exported to MATLAB and meshed using the same algorithm used for the eye model. The gelatine elements were linear continuum elements (type C3D8), Figure 3 Finite element model of the porcine eye globe supported with the gelatine

2.4 Material properties

The cornea, limbus, retina and sclera of all specimens were assumed to follow the stress-strain behaviour reported in the literature for porcine eyes [19, 37]. Following earlier research, the eye model components were assumed to comply with Ogden's hyperelastic strain energy function [38] with the material parameters listed in Table 1 [39].

$$W = \sum_{i=1}^{N} \frac{2\mu_i}{\alpha_i^2}\left(\overline{\lambda_1}^{\alpha_i} + \overline{\lambda_2}^{\alpha_i} + \overline{\lambda_3}^{\alpha_i} - 3\right) + \sum_{i=1}^{N} \frac{1}{D}(J-1)^{2i} \qquad \text{Equation 4}$$

In Equation 4, W is the strain energy per unit volume; N is the function order (taken as 1); μ and α are the strain hardening exponent and the shear modulus, respectively, $\overline{\lambda_k}$ the deviatoric principal stretches = $J^{-1/3} \times \lambda_k$ (k=1, 2, 3), λ_1, λ_2, λ_3 the principal stretches, J = λ_1 λ_2 λ_3. D is a compressibility parameter $= \frac{3(1-2\nu)}{\mu(1+\nu)}$ calculated assuming the tissue was nearly incompressible [40],[41] with a Poisson's ratio, ν, of 0.48 [42, 43]. The material characteristics in the numerical model were validated in earlier studies [19, 25, 36, 44, 45].

The container was modelled as a rigid body to consider the much higher stiffness of its material (steel) compared to that of the tissue components. On the other hand, the gelatine model was given the mechanical properties obtained from the manufacturers and shown in Table 1 Material properties of the different regions of the numerical modelA comparison between two finite element models with no gelatine support and a model with a gelatine support was conducted. The difference in angular displacement ranges between 0.04% and 0.11%.

In consideration of the viscoelastic behaviour of the vitreous reported in the literature [15, 16, 28, 46, 47], the viscoelastic Prony constitutive model was adopted in the analysis [38]:

$$G(t) = G_0\,(t=0) = G_\infty + \sum_{i=1}^{N} G_i\, e^{-t/\tau_i} \qquad \text{Equation 5}$$

where G is the shear relaxation modulus, G_0 and G_∞ are the short and long-term moduli, τ the relaxation time and N is the function order (taken as 1). Values of G_0, G_∞ and $\beta = 1/\tau$ that best represent the behaviour of the vitreous for each specimen, as

observed in the experimental tests, were estimated from the inverse analysis exercise described below.

Table 1 Material properties of the different regions of the numerical model

	Cornea [19]	Limbal region [19]	Anterior sclera [19]	Equatorial region [19]	Posterior sclera [19]	Retina [37]	Gelatine
Constitutive model	Ogden $n=1$	Ogden $n=1$	Ogden $n=1$	Ogden $n=1$	Ogden $n=1$	Ogden $n=2$	Ogden $n=1$
Constitutive model parameters	$\propto = 220.1$ $\mu = 0.0181$	$\propto = 127.2.1$ $\mu = 0.545$	$\propto = 162.3$ $\mu = 0.565$	$\propto = 181.3$ $\mu = 0.642$	$\propto = 134.2$ $\mu = 0.621$	$\propto_1 = 0.00227$ $\mu_1 = 0.0811$ $\propto_2 = 0.00421$ $\mu_2 = 0.0.0652$	$\propto_1 = 0.00239$ $\mu_1 = 0.005$

2.5 Inverse analysis

An inverse analysis exercise was carried out to estimate the viscoelastic properties of the vitreous, G_o, G_∞ and $\beta = 1/\tau$. The inverse analysis is essentially an optimisation process to determine the properties of the vitreous that would lead to the best possible match between the numerical predictions of the displacement at the selected monitoring points (up to 5 in each specimen) and the corresponding experimental measurements. The optimisation was conducted using the Particle Swarm Optimisation (PSO) method, which aimed to reduce the root mean square (RMS) of numerical/experimental mismatch quantified by the following objective function [48-50]:

$$RMS = \sqrt{\frac{1}{P}\sum_{j=1}^{P}\left[\frac{1}{S}\sum_{i=1}^{S}(\theta_{i,j\,Exp} - \theta_{i,j\,Num})^2\right]} \qquad \text{Equation 5}$$

Where P is the number of specimens, S is the total number of displacement levels at which the RMS is calculated, and θ_{Exp} and θ_{Num} respectively represent the experimental and numerical angular displacements at the monitoring points.

After using the inverse analysis to estimate values of the material parameters G_∞, G_o and τ, the exercise was repeated two more times for a randomly selected specimen to test the uniqueness of the material parameter estimations. The analysis was repeated twice while changing the initial values of the three parameters; once with double the initial values and once with half the initial values. The results showed that values of the three parameters changed within 2.8%, 1.9% and 2.9% with changes in the initial values. Throughout these steps, the material model was assumed to have a first-order, $N = 1$, to reduce computation time and reduce the number of variables requiring optimisation.

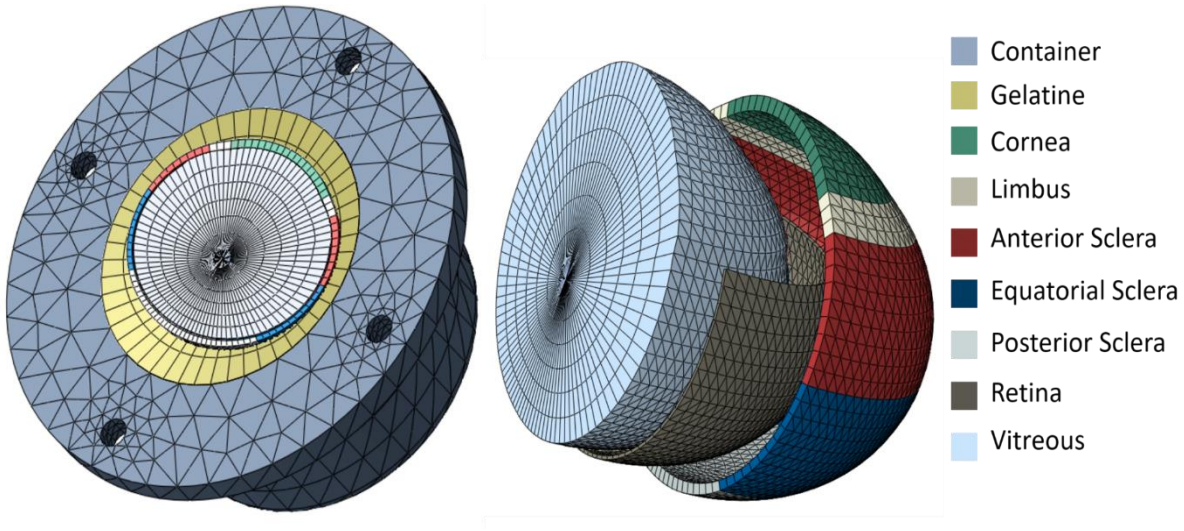

Figure 3 Finite element model of the porcine eye globe supported with the gelatine

3. Results

3.1 Experimental results

Figure 4 shows the rotations recorded at two monitoring points at distances 5.4, 3.8 and 6.4 mm from centre of rotation in three typical specimens tested under 5°, 10° and 15° max displacement, respectively. The rotations are compared to the applied whole eye rotations. In the first test under 5°, the point reached its maximum displacement in the first rotation cycle and reached a steady-state behaviour from the fifth cycle. On the other hand, in the test under 10°, the point reached its maximum displacement in

the fourth cycle and reached a steady-state behaviour from the sixth cycle. In contrast, a steady-state behaviour was evident in the test under 15^{o} from the first rotation cycle with little difference noted in the second and later cycles. The response during the settling period is called the transient response [51], followed by a steady-state response consisting of a sinewave.

Figure 5 illustrates the transient and steady-state responses for the same points in tests with 5^{o} and 15^{o} maximum displacement. The transient state displacements were clearly unstable for the 5^{o} maximum displacement, but this behaviour changed suddenly in the fifth loading cycle indicating the start of the steady-state.

The experimental results show that in tests with eye rotation up to 5^{o}, the displacement monitored in the vitreous did not exceed 4^{o} in the transient-state and 3.2^{o} in the steady-state in all tests. The corresponding maximum displacements in tests with 10^{o} maximum rotation were 6.5^{o} in the transient-state and 4.2^{o} in the steady-state. With 15^{o} maximum rotation, there was no transient-state, while the maximum displacement in the steady-state was 5.6^{o}. The mean ratios between the steady-state displacement and transient-state displacement for all tests with 5^{o} and 10^{o} rotation were 3.7$\pm$0.7 and 6.3$\pm$0.5, respectively.

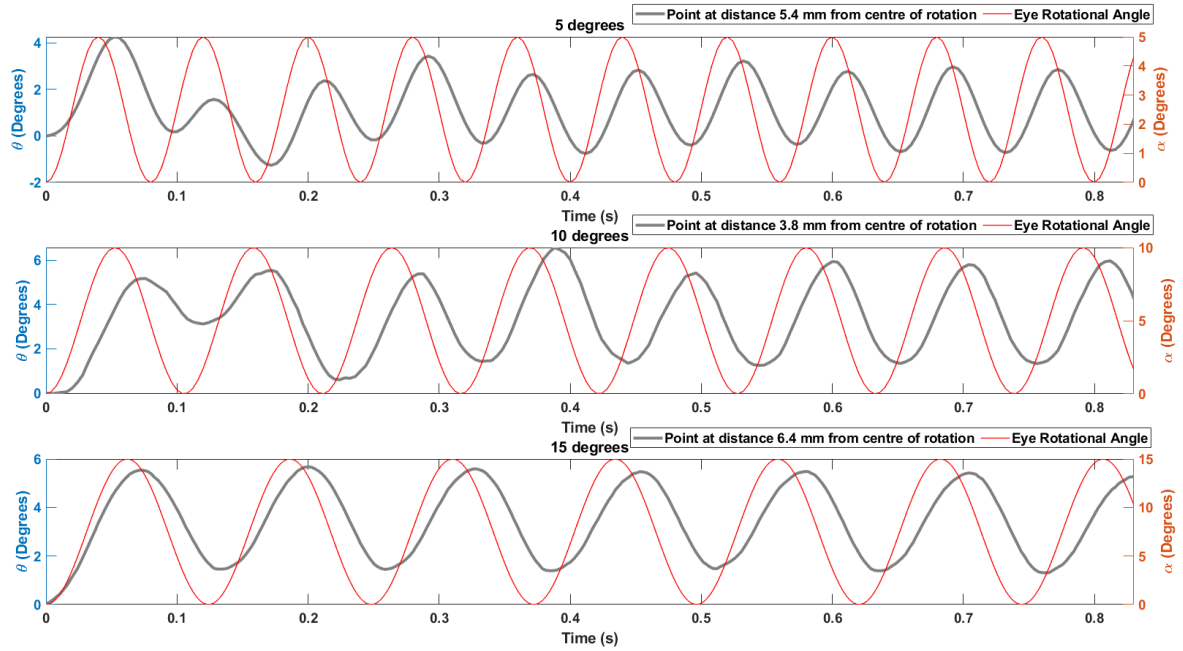

Figure 4 Experimental angular displacement at points with distances of (a) 5.4 mm (b) 3.8 mm and (c) 6.4 mm from centre of rotation in typical tests involving (a) 5^{o} rotation, (b) 10^{o} rotation, and (c) 15^{o} rotation

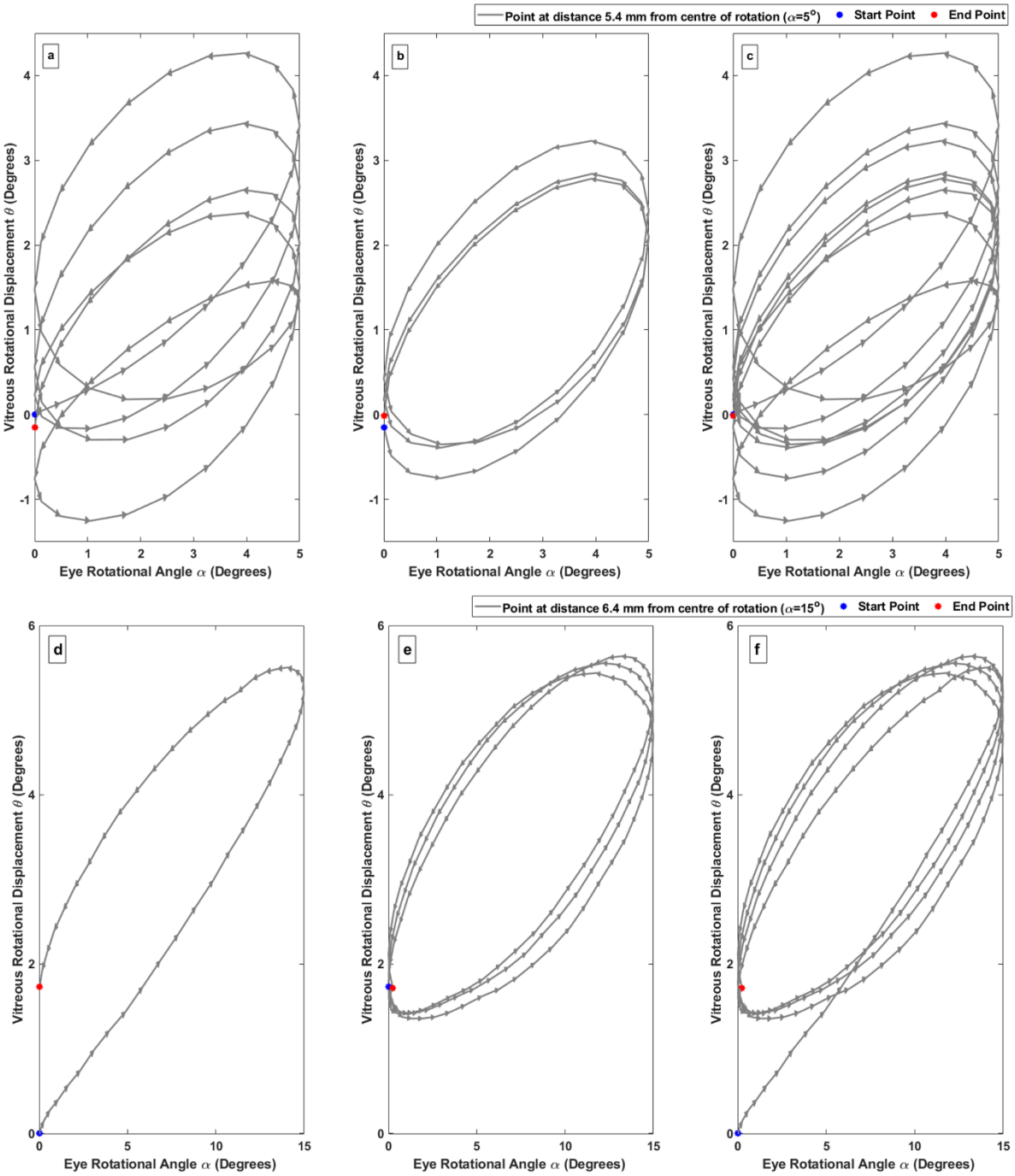

Figure 5 Dynamic behaviour at a point at distance of 5.4 mm from centre of rotation in a typical test under 5° maximum rotations, and a point at distance of 6.4 mm from centre of rotation in a typical test under 15° maximum rotations. (a) and (d) depict the transient-state behaviour under 5° and 15° rotations, respectively; (b) and (e) depict the steady state behaviour; and (c) and (f) depict the transient and steady states combined.

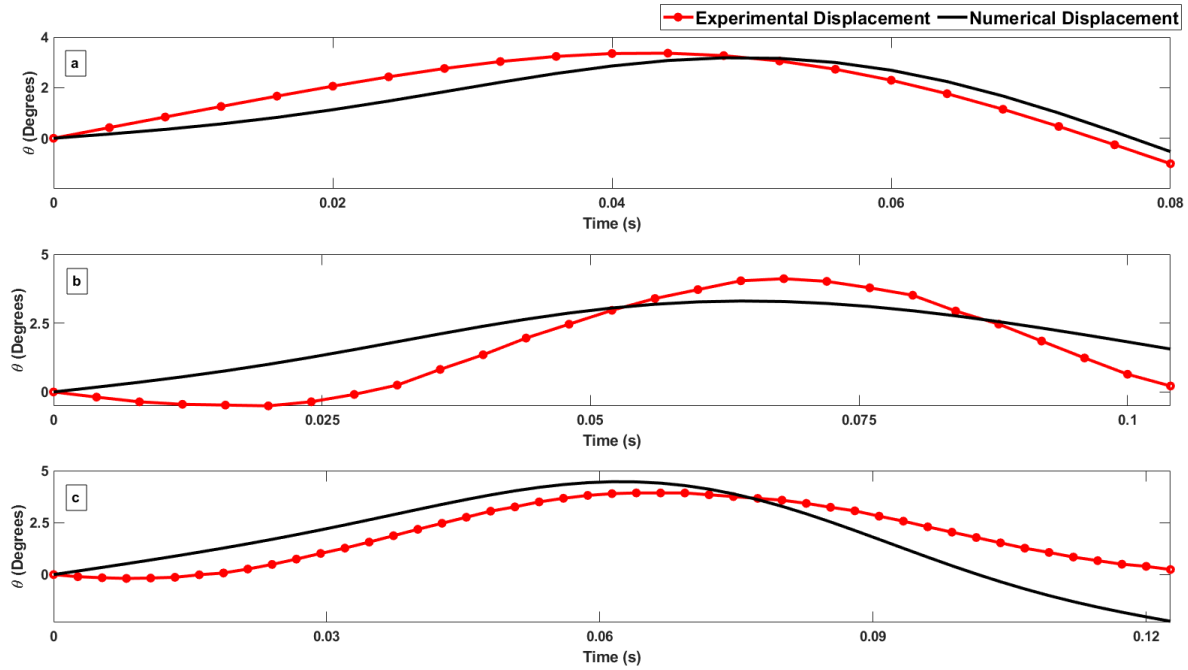

Figure 6 Experimental and numerical displacements at points at 5.4 (a), 3.8 (b), and 6.4 (c) mm in tests with maximum eye rotation of 5^o (a), 10^o (b) and 15^o (c).

3.2 Material parameter estimations

Inverse analysis was used to derive a constitutive model for the vitreous in each eye tested that provided the best possible match (lowest RMS) with the experimentally obtained displacement results. A typical subset of the results is presented in *Figure 6*, for three specimens with maximum rotations of 5^o, 10^o and 10^o, respectively. For all specimens, the mean and standard deviation of the root mean square of experimental/numerical mismatch was 0.98±0.30, and the corresponding material parameters are listed in Table 2.

These values are compared with the results of earlier studies in Table *2* and Figure *7*. While the values of G_∞ and β were intermediate between those reported by Rossi et al and Liu et al, the value of G_0 was below those of the two earlier studies [2, 3].On the other hand, another earlier study by Zimberlin et al ignored the viscoelasticity of the vitreous and reported elastic modulus values. A further assessment of the material properties listed in Table 2 is presented in Figure 7 where a comparison is held

between the numerically-predicted displacements at points at distance of 5.4, 3.8 and 6.4 mm from centre of rotation, for the 5°, 10° and 15° eye rotations, while assuming the material properties listed in Table 2.

Table 2 Vitreous parameters as found numerically and in literature

	Material Parameters			Notes
Current study	$G_o = 2.10 \pm 0.15\ Pa,$	$G_\infty = 0.5 \pm 0.04\ Pa,$	$\beta = 1.2 \pm 0.09\ s^{-1}$	Vitreous remained in eye
Rossi et al, 2011 [3]	$G_o = 10\ Pa,$	$G_\infty = 2\ Pa,$	$\beta = 0.01\ s^{-1}$	Vitreous remained in eye
Liu et al, 2013 [2]	$G_o = 10\ Pa,$	$G_\infty = 0.3\ Pa,$	$\beta = 14.26\ s^{-1}$	Vitreous removed from eye
Zimberlin et al, 2010 [1]	$E = 660\ Pa$			Vitreous remained in eye
Zimberlin et al, 2010 [1]	$E = 120\ Pa$			Vitreous removed from eye

E is the Elastic modulus; G_o Initial shear modulus; G_∞ long-term shear modulus; β viscoelastic decay constant

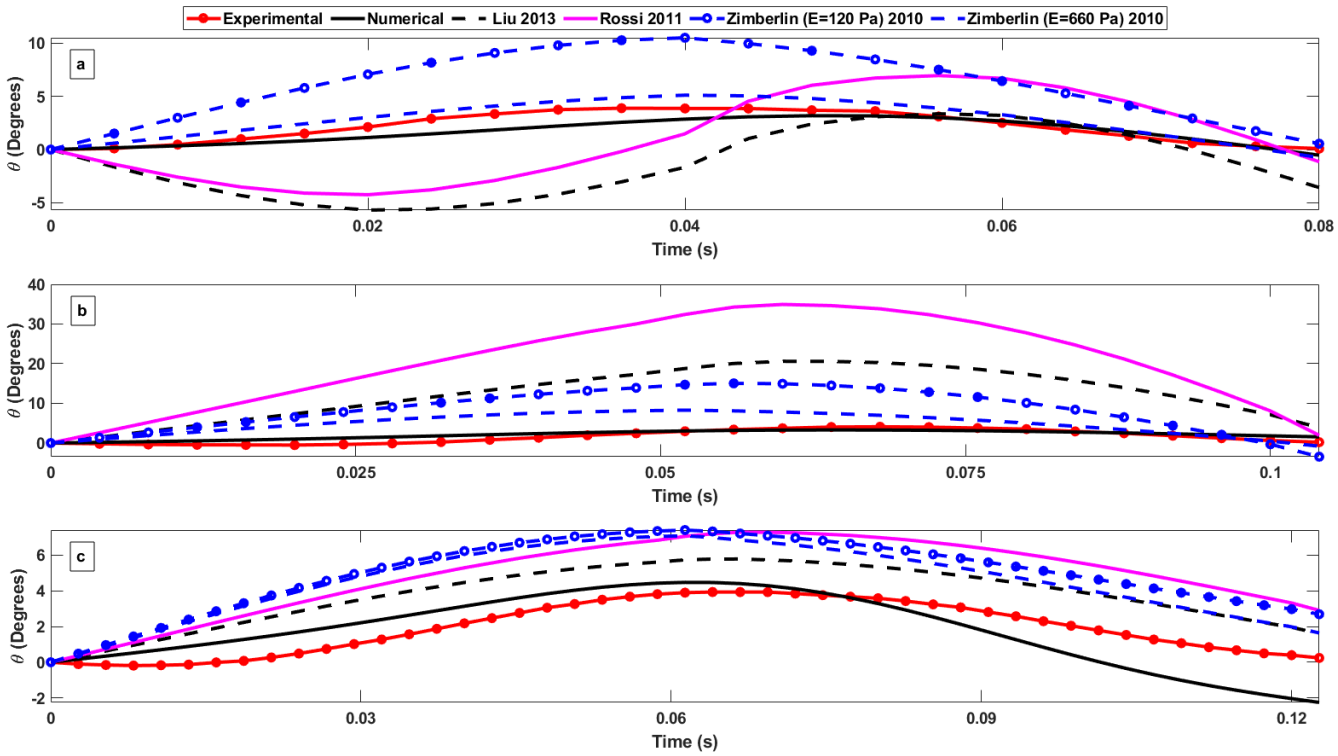

Figure 7 Experimental measurements and numerical predictions of displacements of points at 5.4 (a), 3.8 (b), and 6.4 (c) mm distance from centre of rotation in tests with maximum eye rotation of (a) 5º, (b) 10º, and (c) 15º. Also presented are the numerical predictions of displacements based on the material properties reported in earlier studies.

4 Discussion

The vitreous body has immense importance with regards to the embryogenesis of the eye, the maintenance of its homeostasis and its manifold interactions with neighbouring structures [52]. Deterioration in the vitreous properties can cause various diseases such as the vitreoretinal interface disease, retinal detachment and posterior vitreous detachment [53]. In this study, the properties of the vitreous were measured experimentally while keeping and testing the vitreous in close to its natural physiological conditions. Eye specimens were subjected to dynamic conditions simulating saccade movements, and a numerical inverse analysis was used to estimate the biomechanical properties of the vitreous.

A significant advantage of the experimental method is that it allowed evaluating the properties of the vitreous while keeping the tissue in its natural location, in the posterior chamber, thus avoiding the disturbance that could be caused by extraction. The

specimens were also subjected to dynamic rotations simulating the main loading experienced by the vitreous during eye movement.

Earlier experimental studies have tended to remove the vitreous from the posterior chamber before testing it mechanically – a process that may lead to changes in the mechanical properties. To test this assumption, Zimberlin et al measured the mechanical properties of the vitreous both in its native state and upon removal from the eye [1]. The resulting estimations of the vitreous elasticity modulus were very different; 660 Pa and 120 Pa in the former and latter cases, respectively.

In the same study, Zimberlin et al adopted a cavitation rheology technique, in which a syringe needle was inserted into the posterior chamber to induce elastic instability via slow pressurization [1]. The pressure at which the instability occurred was then related to the mechanical properties of the vitreous. However, the study assumed linear elastic vitreous behaviour and ignored the viscoelastic characteristics of the tissue, and a result its outcome could not be directly compared to the present study. Nevertheless, an indirect comparison could be held while using Zimberlin's elastic modulus in our numerical modelling of the test conditions, which resulted in slightly softer behaviour than that measured experimentally.

In another study by Liu et al [2], the vitreous mechanical properties were obtained from an inverse analysis performed on experimental data. The experimental data was obtained from a rheology test, carried out by Lee et al [54], using a magnetic microrheometer to study small volumes of vitreous samples after extraction from the eye. The viscoelastic model suggested by Liu led to larger predicted displacement – or smaller stiffness – than the experimental results of the present study, especially in the 5º and 10º rotational tests. While the long-term modulus G_∞, reported by Liu was close to the value predicted in the present study, the initial shear modulus G_o, and the decay constant, β, were larger than the values estimated herein due to the vitreous extraction carried out in Liu's study. Moreover, the variation in results is due to Lee et al conducting the experiments after up to 36 hours from extraction after death.

On the other hand, Rossi et al [3] determined the material parameters of the vitreous using multi-objective optimisation performed on the test data of eye impact experiments carried out by Delori et al [24]. The numerical simulation of Rossi et al replicated the dynamic pressure by BB pellet subjected on the eye. The parameters

led to larger displacements than those measured in the current study. The initial shear modulus, the long-term modulus and the decay constant reported by Rossi were more than 4 times larger than the values obtained in this study. The reason behind this large difference could be that the eye was simulated by Rossi to freely move backwards, neglecting the effect of the ballistic gel used by Delori. Also, it could be due to Delori conducting the test only 4 hours after the animal's death without the need to freeze the eye.

The use of porcine eyes is a limitation of the present study. While earlier studies have shown that porcine corneal and scleral tissue had comparable behaviour to that of human tissue [55], there is no explicit evidence that this similarity in behaviour applies to the vitreous. However, the difficulty in getting human eyes in sufficient numbers had made it necessary to rely instead on porcine models, and future work will be needed to verify the applicability of the findings of this research to human tissue. Furthermore, although the specimens were tested within 48 hours post-mortem, it is possible that they had experienced changes in their mechanical properties from their original state, which in turn could have affected the deformation of the vitreous. A further limitation was the need to freeze the tissue before testing, which was necessary for specimen preparation. A recent study found that corneal and scleral tissue experienced negligible changes in mechanical behaviour upon freezing and thawing [56] but there was no evidence that the same effect applied to the vitreous. Moreover, the vitreous parameters were estimated by tracing the displacement of points at different radii from the centre of the posterior chamber. Lee et al [54] indicated that there is a significant difference in the rheological properties of the vitreous regions. However, Zimberlin et al [1], Liu et al [2] and Rossi et al [3] neglected the effect of vitreous heterogeneity when modelling the vitreous. Therefore, future work will be needed to specify whether all three regions differ from each other or not.

In conclusion, the study has investigated experimentally the viscoelasticity of the vitreous humour in order to determine its initial and long-term shear moduli. The emphasis has been on testing and loading the vitreous in close to the natural physiologic conditions, and hence removing some of the possible sources of errors introduced in earlier research. The study produced estimations of the initial shear

modulus and long-term shear modulus that were respectively smaller and larger than reported values.

5. Acknowledgement

A. Aboulatta would like to thank the University of Liverpool for his PhD scholarship award. This research was partly supported by the National Natural Science Foundation of China (No. 11972066) and Key R & D Program of China (No. 2016YFC1103202).

6. References

1. Zimberlin, J.A., J.J. McManus, and A.J. Crosby, *Cavitation rheology of the vitreous: mechanical properties of biological tissue.* Soft Matter, 2010. **6**(15).
2. Liu, X., et al., *Mechanism of traumatic retinal detachment in blunt impact: a finite element study.* J Biomech, 2013. **46**(7): p. 1321-7.
3. Rossi, T., et al., *The pathogenesis of retinal damage in blunt eye trauma: finite element modeling.* Invest Ophthalmol Vis Sci, 2011. **52**(7): p. 3994-4002.
4. Purves D, A.G., Fitzpatrick D, et al., *Anatomy of the Eye*. Neuroscience. Vol. 2nd edition. 2001, Sunderland Sinauer Associates.
5. Sharif-Kashani, P., et al., *Rheology of the vitreous gel: effects of macromolecule organization on the viscoelastic properties.* J Biomech, 2011. **44**(3): p. 419-23.
6. Bishop, P., *Structural macromolecules and supramolecular organisation of the vitreous gel.* Progress in Retinal and Eye Research, 2000. **19**(3): p. 323-344.
7. Sebag, J., *Ageing of the vitreous.* Eye (Lond), 1987. **1 (Pt 2)**: p. 254-62.
8. Romano, M.R., et al., *Retinal Changes Induced by Epiretinal Tangential Forces.* J Ophthalmol, 2015. **2015**: p. 372564.
9. Sodhi, A., et al., *Recent trends in the management of rhegmatogenous retinal detachment.* Surv Ophthalmol, 2008. **53**(1): p. 50-67.
10. Pokki, J., et al., *Measuring localized viscoelasticity of the vitreous body using intraocular microprobes.* Biomed Microdevices, 2015. **17**(5): p. 85.
11. Jacobson, B., T. Dorfman, and P.K. Basu, *Inhibition of Vascular Endothelial Cell Growth and Trypsin Activity by Vitreous* Eye (Lond), 1985. **41**: p. 581 - 595.
12. Foulds, W.S., *Is Your Vitreous Really Necessary? The role of the vitreous in the eye with particular reference to retinal attachment, detachment and the mode of action of vitreous substitutes.* Eye (Lond) 1987. **1**: p. 641-664.
13. Stein, J., et al., *Adverse Events After Pars Plana Vitrectomy Among Medicare Beneficiaries.* Arch Ophthalmol, 2009. **127**(12): p. 1656–1663.
14. Ryan, E.H., Jr and R.A. Mittra, *Scleral Buckling vs Vitrectomy: The Continued Role for Scleral Buckling in the Vitrectomy Era.* Archives of Ophthalmology, 2010. **128**(9): p. 1202-1205.
15. Bettelheim, F.A. and T.J.Y. Wang, *Dynamic Viscoelastic Properties of Bovine Vitreous.* Exl: Eye Res, 1976. **23**: p. 435-441.
16. Zimmerman, R.L., *In vivo measurements of the viscoelasticity of the human vitreous humor.* BIOPHYS. J., 1980. **29**: p. 539-544.
17. James, A., et al., *Study of Vitreous Liquifaction by NMR Spectroscopy and Imaging.* Invest Ophthalmol Vis Sci, 1985. **26**: p. 692-697.
18. Nickerson, C.S., et al., *Rheological properties of the vitreous and the role of hyaluronic acid.* J Biomech, 2008. **41**(9): p. 1840-6.

19. Whitford, C., et al., *Ex vivo testing of intact eye globes under inflation conditions to determine regional variation of mechanical stiffness.* Eye Vis (Lond), 2016. **3**: p. 21.
20. Abyaneh, M.H., et al., *A hybrid approach to determining cornea mechanical properties in vivo using a combination of nano-indentation and inverse finite element analysis.* Journal of the Mechanical Behavior of Biomedical Materials, 2013. **27**: p. 239-248.
21. Nguyen, T.D. and B.L. Boyce, *An inverse finite element method for determining the anisotropic properties of the cornea.* Biomech Model Mechanobiol, 2011. **10**(3): p. 323-37.
22. Zhang, K., et al., *An inverse method to determine the mechanical properties of the iris in vivo.* BioMedical Engineering OnLine, 2014. **13**(1): p. 66.
23. Esposito, L., et al., *Modelling human eye under blast loading.* Comput Methods Biomech Biomed Engin, 2015. **18**(2): p. 107-15.
24. Delori, F., O. Pomerantzeff, and M.S. Cox, *Deformation of the globe under high-speed impact: it relation to contusion injuries.* Invest Ophthalmol, 1969. **8**(3): p. 290-301.
25. Vroon, J., et al., *Numerical study of the effect of head and eye movement on progression of retinal detachment.* Biomech Model Mechanobiol, 2018. **17**(4): p. 975-983.
26. Fisher, L.K., et al., *Gaze-evoked deformations of the optic nerve head in thyroid eye disease.* bioRxiv, 2020: p. 2020.03.19.999706.
27. Karami, A. and M. Eghtesad, *Simulation of Active Eye Motion Using Finite Element Modelling.* Latin American Journal of Solids and Structures, 2018. **15**.
28. David, T., et al., *A model for the fluid motion of vitreous humour of the human eye during saccadic movement.* Physics in Medicine & Biology, 1998. **43**(6): p. 1385–1399.
29. Kapnisis, K., M.V. Doormaal, and C. Ross Ethier, *Modeling aqueous humor collection from the human eye.* J Biomech, 2009. **42**(15): p. 2454-7.
30. Sinha Roy, A. and W.J. Dupps, Jr., *Effects of altered corneal stiffness on native and postoperative LASIK corneal biomechanical behavior: A whole-eye finite element analysis.* J Refract Surg, 2009. **25**(10): p. 875-87.
31. Myers, K.M., et al., *The inflation response of the posterior bovine sclera.* Acta Biomaterialia, 2010. **6**(11): p. 4327-4335.
32. Boyce, B.L., et al., *Full-field deformation of bovine cornea under constrained inflation conditions.* Biomaterials, 2008. **29**(28): p. 3896-3904.
33. Lancaster, W., *Fifty Years' Experience in Ocular Motility.* Am J Ophthal, 1941. **24**: p. 741-748.
34. Yarbus, A.Y., *Eye movements and vision*. 1967, New York: Plenum Press.
35. Nooshin, H., *Space structures and configuration processing.* Progress in Structural Engineering and Materials 1998. **1**(3): p. 329336.
36. Elsheikh, A. and D. Wang, *Numerical modelling of corneal biomechanical behaviour.* Comput Methods Biomech Biomed Engin, 2007. **10**(2): p. 85-95.
37. Qian, X., K. Zhang, and Z. Liu, *A method to determine the mechanical properties of the retina based on an experiment in vivo.* Biomed Mater Eng, 2015. **26 Suppl 1**: p. S287-97.
38. Haojie, M., *Basic Finite Element Method as Applied to Injury Biomechanics*. 2018: Academic Press.
39. Ogden, R.W., *Large deformation isotropic elasticity: on the correlation of theory and experiment for compressible rubberlike solids.* Royal Society, 1972. **328**(1575).
40. Grupcheva, C.N., et al., *In vivo confocal microscopy of corneal epithelial ingrowth through a laser in situ keratomileusis flap buttonhole.* J Cataract Refract Surg, 2001. **27**(8): p. 1318-22.
41. Dhaliwal, D.K., et al., *Valacyclovir inhibition of recovery of ocular herpes simplex virus type 1 after experimental reactivation by laser in situ keratomileusis.* J Cataract Refract Surg, 2001. **27**(8): p. 1288-93.
42. Yu, J.G., et al., *Assessment of corneal biomechanical behavior under posterior and anterior pressure.* J Refract Surg, 2013. **29**(1): p. 64-70.
43. Bao, F., et al., *Effects of diabetes mellitus on biomechanical properties of the rabbit cornea.* Exp Eye Res, 2017. **161**: p. 82-8.

44. Elsheikh, A., et al., *Regional variation in the biomechanical properties of the human sclera.* Experimental Eye Research, 2010. **90**(5): p. 624-633.
45. Elsheikh, A., et al., *Numerical study of the effect of corneal layered structure on ocular biomechanics.* Curr Eye Res, 2009. **34**(1): p. 26-35.
46. Yoon, S., et al., *Spatial Variations of Viscoelastic Properties of Porcine Vitreous Humors.* Correspondence, 2013. **60**(11): p. 2453-2460.
47. Silva, A.F., M.A. Alves, and M.S.N. Oliveira, *Rheological behaviour of vitreous humour.* Rheologica Acta, 2017. **56**(4): p. 377-386.
48. Chen, J., et al., *Reliability design optimization of composite structures based on PSO together with FEA.* Chinese Journal of Aeronautics, 2013. **26**(2): p. 343-349.
49. Elias de Oliveira, M., et al., *A multi-criteria decision support for optimal instrumentation in scoliosis spine surgery.* Structural and Multidisciplinary Optimization, 2011. **45**(6): p. 917-929.
50. Liu, X., H. Liu, and H. Duan, *Particle swarm optimization based on dynamic niche technology with applications to conceptual design.* Advances in Engineering Software, 2007. **38**(10): p. 668-676.
51. Bechlioulis, C.P. and G.A. Rovithakis, *Adaptive control with guaranteed transient and steady state tracking error bounds for strict feedback systems.* Automatica, 2009. **45**(2): p. 532-538.
52. Schulz, A., et al., *Age-Related Loss of Human Vitreal Viscoelasticity.* Transl Vis Sci Technol, 2019. **8**(3): p. 56.
53. Foos, R.Y. and N.C. Wheeler, *Vitreoretinal juncture. Synchysis senilis and posterior vitreous detachment.* Ophthalmology, 1982. **89**(12): p. 1502-1512.
54. Lee, B., M. Litt, and G. Buchsbaum, *Rheology of the vitreous body. Part I: Viscoelasticity of human vitreous.* Biorheology, 1992. **29**(5-6): p. 521-33.
55. Olsen, T.W., et al., *Porcine Sclera: Thickness and Surface Area.* Investigative Ophthalmology & Visual Science, 2002. **43**(8): p. 2529-2532.
56. Abass, A., et al., *Effect of freezing and thawing on the biomechanical characteristics of porcine ocular tissues.* J Biomech, 2019. **87**: p. 93-99.